PERGAMON

International Journal of Plasticity 18 (2002) 1649–1659

INTERNATIONAL JOURNAL OF Plasticity

www.elsevier.com/locate/ijplas

On perfectly plastic flow in porous material

T.I. Zohdi*,[a], M. Kachanov[b], I. Sevostianov[c]

[a]*Department of Mechanical Engineering, 6195 Etcheverry Hall, University of California, Berkeley, CA 94720-1740, USA*

[b]*Department of Mechanical Engineering, Tufts University, Medford, MA 02153, USA*

[c]*Department of Mechanical Engineering, New Mexico State University, PO Box 30001, Las Cruces, NM 88003, USA*

Received in final revised form 15 December 2001

Abstract

Experimental observations suggest that for perfectly-plastic materials containing pores, the (small) strain at which significant macroscopic yielding occurs is relatively insensitive to porosity, for volume fractions below approximately 15–20% (although the yield stress drops significantly with increasing porosity). Another observation is that, at these porosity levels, the stress–strain curve remains approximately linear almost up to the yield point. Based on these observations, Sevostianov and Kachanov constructed yield surfaces that explicitly reflect the shapes of the pores and their orientation. The underlying microscale mechanism is that local plastic "pockets" near pores blunt the stress concentrations; as a result, they remain limited in size and well contained in the elastic field until they connect and almost the entire matrix plasticizes within a narrow interval of stresses that can be idealized as the yield point. The present paper provides direct insight into the micromechanics of poroplasticity through direct microscale numerical simulation. Besides confirming the basic microscale mechanism, these simulations reveal that the reduction of the macroscopic poroplastic yield stress is approximated quite closely by $1-v_2$ times the dense nonporous yield stress, where v_2 is the volume fraction of the pores. © 2002 Published by Elsevier Science Ltd.

Keywords: Porous media; Micro/macro yield

1. Introduction

Research in plasticity of porous materials has, at least, a 40 year history. This research appears to have proceeded in two primary directions: (A) plasticity at small overall strains, in particular, determination of the macroscopic yield surface in stress

* Corresponding author. Tel.: +1-510-642-9172; fax: +1-510-642-6163.
E-mail address: zohdi@newton.berkeley.edu (T.I. Zohdi).

0749-6419/02/$ - see front matter © 2002 Published by Elsevier Science Ltd.
PII: S0749-6419(02)00005-0

space, accounting for porosity, in the cases when such a surface can be clearly identified and (B) void growth and coalescence at much larger overall strains. Problem (B) has been a subject of intensive investigations in recent years, that stem mostly from the analysis of Gurson (1977). A particularly lucid analysis of Gurson's model, and its early extensions can be found in Mear (1990). For the latest developments of the model, and its wide range of applications, we refer the reader to Pardoen and Hutchinson (2000), Horstmeyer et al. (2000), Khan and Zhang (2000), Kharaishi et al. (2001), Gu et al. (2001) and Mähler et al. (2001). The present work focuses on problem (A), of which some theoretical aspects, in particular explicit construction of the yield surface in terms of the pore geometry, have been developed in Sevostianov and Kachanov (2001). Earlier rigid–plastic analyses, restricted to dilute pore concentration levels, is attributed to Lee and Mear (1991) and Yee and Mear (1996). In those analyses, pore shape geometry of rigid–perfectly plastic materials containing voids (and rigid inclusions) were investigated via dilute methods. Related works, however investigating the effects of orientation can be found in Qui and Weng (1993) and Nagayaki et al. (1993). As far as the small strain plasticity of porous materials at *non-dilute*, *finite* levels is concerned, other earlier works focused mainly on the phenomenological modeling of the observed behavior, in particular, the dependence of the macroscopic yield on the first invariant of stress tensor. In this framework, yield surfaces for porous materials appear to be first discussed by Skorokhod (1965) in relation to powder metallurgy. Kuhn and Downey (1971) and Green (1972) independently proposed, on phenomenological grounds, the yield conditions (and the equations of plastic deformation) for porous materials. Their yield conditions depend not only on the intensity of shear stresses but on the first invariant of stress tensor as well. Shima and Oyane (1976) and Shtern (1981), estimated the constants entering the yield conditions in the mentioned works from experimental data. Related studies can be found in Lee (1988). For an extensive review of literature related to the powder metallurgy applications, see Olevsky (1998).

Recent developments in technology of porous materials manufacturing (see, for example, Shapovalov, 1993; Shapovalov and Timchenko, 1993; Kee et al., 1998; Everett, 1998) created a need for deeper understanding of the relation between the plastic behavior and the microstructure. In this context, a micromechanical model was recently suggested by Sevostianov and Kachanov (2001). They assumed perfectly plastic behavior of the matrix and constructed a model based on the following experimental observations concerning materials with well defined yield surfaces (Wang et al., 1996; Da Silva and Ramesh 1997a,b; Kee et al., 1998):

- The existence of a clearly identifiable point of the macroscopic yield, for porosities up to 20%, that separates the stage of a more or less linear stress–strain relation from the phase of macroscopically perfectly plastic flow. This suggests, albeit in an indirect way, that the entire matrix is fully, or almost fully, plasticized in the flow phase, so that the field of stress deviator is almost homogeneous in the matrix. Note that, for a material with pores—stress concentrators—such a picture may not be intuitively obvious. From the physical point of view, this uniformity of the field of the stress deviator in the

plastic phase can be explained as follows. Although local plastic "pockets" near pores appear at low levels of applied loads, they blunt the stress concentrations to such an extent that further increases in loading produce only a very limited growth of their size. These plastic "pockets" remain well embedded into the elastic phase. Then, within a narrow interval of applied loads—that can be idealized as a point—a transition to the fully (or almost fully) plasticized matrix takes place. This picture differs from the highly non-uniform stress field for a *hardening* material. This difference seems natural, since stress "blunting" in a strain hardening material is substantially less pronounced, so that the growth of local plastic zones continues to be enhanced by the stress concentrations, as the applied loads increase, leading, possibly, to localizations.

- Since the stress deviator at macroscopic yield is approximately uniform over the matrix, it is equal to its average over the matrix. On the other hand, as mentioned above, the transition from the mostly elastic state (with local plasticity "pockets" well embedded into the elastic field) to the yield point occurs in a narrow interval of the applied loads that precedes the yield point. Therefore, the value of the mentioned average can be estimated from the *elastic* solutions.

Experimental observations show that the macroscopic strain at the onset of yield is relatively insensitive to volume fraction of voids (Wang et al., 1996; Da Silva and Ramesh, 1997a,b; Kee et al., 1998). Note, that the materials in these investigations were almost perfectly plastic (no noticeable hardening). Generalizing these observations, Sevostianov and Kachanov (2001) postulated that, at the macroscopic yield, the strain at yield is constant and can, therefore, be estimated from its value ε_0 for the dense material (material without pores). In a porous material, the given constant level of strain corresponds to reduced (as compared to the dense material) stresses, thus altering the yield surface. Calculating this reduction from the elastic solutions produces a yield surface that explicitly reflects pore shapes and orientations. Such calculations were done on the basis of the technique developed by Kachanov et al. (1994). The purpose of the present communication is to shed light on the microscale mechanisms involved. Two primary results are as follows:

- The onset of the macroscopic yield indeed occurs in a narrow interval of the applied stresses, so that the macroscopic yield surface in the stress space is clearly identifiable.
- At the onset of the macroscopic yield, the field of the stress deviator is almost uniform in the matrix (thus justifying identification of the macroscopic yield in terms of the average, over the matrix, stress deviator). As a consequence, the numerical results suggest that the macroscopic yield stress can simply be scaled by the $(1-v_2)$, where v_2 is the pore volume fraction.

In the text to follow, we outline a scheme of numerical microscale simulations for a general microheterogeneous material that may contain multiple inclusions or pores, and then apply the approach to investigate the progressive plastification of porous material microstructure.

2. Microscale elasto-plastic numerical simulations

We consider a micro-heterogeneous material with pointwise mechanical properties characterized by an elasticity tensor that is piecewise continuous. Of interest is the effective stress–strain relationship, i.e. the relationship between averages over a representative volume element (RVE). The material on the microscale is assumed to obey the classical equations of elastio-plastic behavior. The existence of a closed surface in the space of principal stresses is assumed, where within the boundary the behavior of the material is elastic, and on it, it is inelastic. The equation for this surface is $\Psi(\boldsymbol{\sigma},\ \boldsymbol{\varphi})=0$, where $\boldsymbol{\varphi}$ are internal variables ($\boldsymbol{\varphi}\stackrel{\text{def}}{=}\{\varphi_i,\ \ldots,\ \varphi_N\}$) that, generally, change with plastic deformation. As usual, this relation is split according to $\Psi(\boldsymbol{\sigma},\ \boldsymbol{\varphi})=\mathcal{M}(\boldsymbol{\sigma})-\mathcal{K}(\boldsymbol{\varphi})=0$, where $\mathcal{M}$, is a measure of the internal fields and $\mathcal{K}$ is a constraint. Generally, the strains depend on these variables in addition to stress, and temperature, where for each internal variable $\dot{\varphi}_i=\mathcal{F}_i(\boldsymbol{\sigma},\ \boldsymbol{\varphi})$, $i=1,..,N$, is the evolution or "rate" equation. The manner in which the internal variables enter into Ψ is defined as the hardening or softening rule. We have the standard loading/unloading conditions: (I) if inside the yield surface, $\Psi<0$, or on the yield surface, $\Psi=0$, with a negative loading rate, $\frac{\partial\Psi}{\partial\boldsymbol{\sigma}}:\dot{\boldsymbol{\sigma}}<0$, then the response is elastic or (II) if on the yield surface, $\Psi=0$ and a positive loading rate, $\frac{\partial\Psi}{\partial\boldsymbol{\sigma}}:\dot{\boldsymbol{\sigma}}\geqslant 0$, then the response is inelastic. Case (I) indicates that the stress state is below the criteria or is being unloaded in that direction from a critical state, while case (II) indicates the critical state is met, and the loading stress increasing. For infinitesimal deformations, the strains are usually split in the following manner, $\boldsymbol{\varepsilon}=\boldsymbol{\varepsilon}_e+\boldsymbol{\varepsilon}_p$, where $\boldsymbol{\varepsilon}_e$ and $\boldsymbol{\varepsilon}_p$ are the elastic and plastic strains respectively. One of the simplest models is to choose $\varphi=\sqrt{\boldsymbol{\varepsilon}_p:\boldsymbol{\varepsilon}_p}$ as the only internal variable, where inelastic effects are coupled through the stress and the constraint $\mathcal{K}(\varphi)=C_1+C_2\varphi^{C_3}$, where C_1, C_2 and C_3 are given constants. A natural and easy way to represent an evolution law is $\dot{\boldsymbol{\varepsilon}}_p=\dot{\lambda}\frac{\partial\Pi}{\partial\boldsymbol{\sigma}}$, where Π is a so-called flow potential, and where $\dot{\lambda}$ is a nonnegative scalar function. Clearly, in case (I) we have $\dot{\Psi}=0$ which implies $\dot{\boldsymbol{\varepsilon}}_{\mathrm{p}}=0$ while for case (II), we have $\dot{\Psi}\geqslant 0$ which implies $\dot{\boldsymbol{\varepsilon}}_{\mathrm{p}}\neq\boldsymbol{0}$. The "rate" equations are $(\mathrm{d}\varepsilon_p)_{ij}=\mathrm{d}\lambda h_{ij}$, $h_{ij}=\frac{\partial\Pi}{\partial\sigma_{ij}}$. If $\Psi=\Pi$, the flow is called associated, i.e. associated with the yield surface. One usually makes a dilatational–deviatoric split of the form $g(\boldsymbol{\sigma})=\eta_1\frac{\mathrm{tr}\boldsymbol{\sigma}}{3}\mathbf{1}+\eta_2\left(\boldsymbol{\sigma}-\frac{\mathrm{tr}\boldsymbol{\sigma}}{3}\mathbf{1}\right)$, where $\mathcal{M}(\boldsymbol{\sigma})=(g(\boldsymbol{\sigma}):g(\boldsymbol{\sigma}))^{\frac{1}{2}}$, and where η_1 and η_2 are positive weights. Therefore, $(g(\boldsymbol{\sigma}):g(\boldsymbol{\sigma}))^{\frac{1}{2}}-\left(C_1+C_2\varphi^{C_3}\right)=0$ is the constraint to satisfy. It is clear that a variety of inelastic effects can be modeled by judicious choice of η_1 and η_2. The usual choice is $\eta_1=0$. For perfect plasticity, with no work hardening, C_1 is understood to be the yield stress, and $C_2=0$. For a review, see Khan and Huang (1995).

For the class of problems of interest, namely perfect plasticity with an irregular microstructure, a global fixed-point/local Newton approach, as opposed to a complete global Newton/local Newton type, which require global tangents, is preferred. Primarily, this is because of the necessity of using small load steps to capture the small length scales inherent in the micro-macro mechanical simulations, as well as the possibility of zero tangents, inherent when employing models of perfect plasticity. We employ the following somewhat standard superscript notation (1) L is the load increment counter, (2) I is the global solve counter (within a load increment)

and $-(3)$ i is the local Newton internal iteration counter (within a global solve). It is assumed that the stress $\boldsymbol{\sigma}^{L-1,\cdot,\cdot}$ and inelastic strain $\boldsymbol{\varepsilon}_p^{L-1,\cdot,\cdot}$, the values at the end of load increment $L-1$, have been determined to sufficient accuracy so that $\Psi(\boldsymbol{\sigma}^{L-1,\cdot,\cdot}, \boldsymbol{\varepsilon}_p^{L-1,\cdot,\cdot} \leqslant \text{tol})$, $\forall \boldsymbol{x} \in \Omega$, at this loading level. Now the load is incremented, and thus $\Delta\boldsymbol{\varepsilon}$ (via the external load) is changed, and the stress increment is initially assumed to produce a purely elastic strain increment ($\Delta\boldsymbol{\varepsilon}_e^{L,\cdot,\cdot}$), by solving the following variational boundary value problem: Find $\mathbf{u}^L \in \mathbf{U}(\Omega)$, $\boldsymbol{u}^L\big|_{\Gamma_u} = \mathbf{d}^L$, such that $\forall \boldsymbol{v} \in \boldsymbol{V}(\Omega)$, $\boldsymbol{v}|_{\Gamma_u} = \boldsymbol{0}$, $\int_\Omega \nabla \boldsymbol{v} : \boldsymbol{\sigma}^L \mathrm{d}\Omega = \int_\Omega \boldsymbol{f}^L \cdot \boldsymbol{v} \mathrm{d}\Omega + \int_{\Gamma_t} \boldsymbol{t}^L \cdot \boldsymbol{v} \mathrm{d}A$, where $\boldsymbol{\sigma}^L = \boldsymbol{\sigma}^{L,\cdot} \stackrel{\text{def}}{=} \mathbb{E}: (\boldsymbol{\varepsilon}^{L,\cdot,\cdot} - \boldsymbol{\varepsilon}_p^{L-1,\cdot,\cdot})$, where $\boldsymbol{\varepsilon}^{L,\cdot,\cdot} \stackrel{\text{def}}{=} \boldsymbol{\varepsilon}^{L-1,\cdot,\cdot} + \Delta\boldsymbol{\varepsilon}_e^{L,\cdot,\cdot}$, where $\mathbf{U}(\Omega)$ and $\mathbf{V}(\Omega)$ are spaces of admissible trial and test functions and where $\mathbf{f}^L$, $\mathbf{t}^L$ and $\mathbf{d}^L$ are the incrementally applied loads. If $\Psi(\boldsymbol{\sigma}^{L,\cdot,\cdot}, \boldsymbol{\varepsilon}_p^{L-1,\cdot,\cdot}) \leqslant \text{tol}$, $\forall \boldsymbol{x} \in \Omega$, then the predictor is assumed correct. If $\Psi(\boldsymbol{\sigma}^{L,\cdot,\cdot}, \boldsymbol{\varepsilon}_p^{L-1,\cdot,\cdot}) > \text{tol}$, $\forall \boldsymbol{x} \in \Omega$, then some inelasticity has occurred and must be determined. Following the usual procedure for problems with constraints, within a load increment L, containing a global (fixed-point) solution process, the Newton/Raphson scheme is used to satisfy the constraints locally. *The displacement field, and consequently the strain field, are frozen during these local iterations*. The return mapping process is a procedure to satisfy the constraints. We have $\Delta\boldsymbol{\varepsilon}_p^{L,I,i} = \Delta\lambda^{L,I,i}\boldsymbol{h}(\boldsymbol{\sigma}^{L,I,i})$ and $\Delta\varphi^{L,I,i} = \Delta\lambda^{L,I,i}\|\boldsymbol{h}(\boldsymbol{\sigma}^{L,I,i})\|$, where $\mathbf{h} = \frac{\partial\Psi}{\partial\boldsymbol{\sigma}} = 2\frac{\partial g(\boldsymbol{\sigma})}{\partial\boldsymbol{\sigma}} \cdot g(\boldsymbol{\sigma})$. The constraint condition is that the stress must be pushed back to the constraint surface. We have, by the chain rule of calculus, during the local iterations

$$\Psi^{L,I,i} \approx \Psi^{L,I,i-1} + \left.\frac{\partial\Psi}{\partial\boldsymbol{\sigma}}\right|_{\sigma^{L,I,i-1}} : \left(\boldsymbol{\sigma}^{L,I,i} - \boldsymbol{\sigma}^{L,I,i-1}\right) + \left.\frac{\partial\Psi}{\partial\varphi}\right|_{\varphi^{L,I,i-1}} \left(\varphi^{L,I,i} - \varphi^{L,I,i-1}\right). \tag{1}$$

Since $\mathrm{d}\varphi = \mathrm{d}\sqrt{(\boldsymbol{\varepsilon}_p : \boldsymbol{\varepsilon}_p)} = \frac{1}{2}(\boldsymbol{\varepsilon}_p : \boldsymbol{\varepsilon}_p)^{-\frac{1}{2}}(\boldsymbol{\varepsilon}_p : \mathrm{d}\boldsymbol{\varepsilon}_p + \mathrm{d}\boldsymbol{\varepsilon}_p : \boldsymbol{\varepsilon}_p) = \frac{\mathrm{d}\lambda\boldsymbol{\varepsilon}_p:\boldsymbol{h}}{\varphi}$,

$$\Psi^{L,I,i-1} - \left.\frac{\partial\Psi}{\partial\boldsymbol{\sigma}}\right|_{\sigma^{L,I,i-1}} : \mathbb{E} : \Delta\lambda^{L,I,i}\boldsymbol{h}(\boldsymbol{\sigma}^{L,I,i}) + \left.\frac{\partial\Psi}{\partial\varphi}\right|_{\varphi^{L,I,i-1}} \frac{\Delta\lambda^{L,I,i}\boldsymbol{\varepsilon}_p^{L,I,i} : \boldsymbol{h}^{L,I,i}}{\varphi^{L,I,i}} \approx 0. \tag{2}$$

Solving for $\Delta\lambda^{L,I,i}$, we obtain

$$\Delta\lambda^{L,I,i} \approx \frac{\Psi^{L,I,i-1}}{\left.\frac{\partial\Psi}{\partial\boldsymbol{\sigma}}\right|_{\sigma^{L,I,i-1}} : \mathbb{E} : \boldsymbol{h}(\boldsymbol{\sigma}^{L,I,i}) - \left.\frac{\partial\Psi}{\partial\varphi}\right|_{\varphi^{L,I,i-1}} \frac{\boldsymbol{\varepsilon}_p^{L,I,i}:\boldsymbol{h}^{L,I,i}}{\varphi^{L,I,i}}} \tag{3}$$

Within each load increment, the system is resolved until the constraints and equilibrium are satisfied.[1] Algorithmically the system can be solved by, for example in displacement control

[1] The global violation of the constraints is $\|\mathcal{M} - \mathcal{K}\|_C \stackrel{\text{def}}{=} \frac{1}{|\Omega|}\int_\Omega \frac{\max(\mathcal{M},\mathcal{K}) - \mathcal{K}}{\mathcal{K}} \mathrm{d}\Omega$.

$$
\begin{aligned}
&(1)\ INCREMENT\ \ LOAD: \boldsymbol{u}^{L}\big|_{\Gamma_u} \stackrel{\text{def}}{=} \boldsymbol{u}^{L-1}\big|_{\Gamma_u} + \delta\boldsymbol{u}^{L}\big|_{\Gamma_u} \\
&\quad ASSUME\ \ PURELY\ \ ELASTIC\ \ INCREMENTAL\ \ RESPONSE \\
&\quad \boldsymbol{\sigma}^{L,I,i=0} = \mathbb{E} : \left(\boldsymbol{\varepsilon}^{L,I} - \boldsymbol{\varepsilon}_p^{L,I}\right) \qquad \left(\boldsymbol{\varepsilon}_p^{L,I} = \boldsymbol{\varepsilon}_p^{L,I-1}\right) \\
&\quad I = 1, \ \ \Delta\boldsymbol{\varepsilon}_p^{L,I} = \boldsymbol{0} \ \forall\ \boldsymbol{x} \in \Omega \\
&(2)\ GLOBALLY\ \ COMPUTE: \boldsymbol{u}^{L,I} \\
&\quad IF\ \left(\left\|\mathcal{M}^{L,I} - \mathcal{K}^{L,I}\right\|_C \leqslant TOL\right) THEN\ \ GOTO\ (3) \\
&\quad IF\ \left(\left\|\mathcal{M}^{L,I} - \mathcal{K}^{L,I}\right\|_C > TOL\right) THEN\ \ FOR\ \ EACH\ \boldsymbol{x} \in \Omega : (i = 1) \\
&\qquad IF\ \left(\mathcal{M}^{L,I}\mathcal{K}^{L,I}\right) THEN\ \ COMPUTE\ \boldsymbol{\varepsilon}_p^{L,I,i}\ \ FROM: \\
&\qquad \Delta\lambda^{L,I,i} = \frac{\Psi^{L,I,i-1}}{\frac{\partial\Psi}{\partial\boldsymbol{\sigma}}\big|_{\sigma^{L,I,i-1}} : \mathbb{E} : \boldsymbol{h}(\boldsymbol{\sigma}^{L,I,i}) - \frac{\partial\Psi}{\partial\varphi}\Big|_{\varphi^{L,I,i-1}} \frac{\boldsymbol{\varepsilon}_p^{L,I,i}\boldsymbol{h}^{L,I,i}}{\varphi^{L,I,i}}} \\
&\qquad \forall\ \boldsymbol{x} \in \Omega : \Delta\boldsymbol{\varepsilon}_p^{L,I,i} = \Delta\lambda^{L,I,i}\boldsymbol{h}^{L,I,i} \ \Rightarrow\ \boldsymbol{\varepsilon}_p^{L,I,i} = \boldsymbol{\varepsilon}_p^{L,I} + \Delta\boldsymbol{\varepsilon}_p^{L,I,i} \\
&\qquad REPEAT\ \ UNTIL\ \ CONSTRAINTS\ \ ARE\ \ SATISFIED \\
&(3)\ UPDATE\ \ ALL\ \boldsymbol{\varepsilon}_p^{L,I,i+1}; \ \ I = I + 1; \ \ AND\ \ GOTO\ (2) \\
&L = L + 1\ \ AND\ \ GOTO\ (1).
\end{aligned}
\tag{4}
$$

Typically the convergence of such algorithms is inversely dependent on the load step size. Therefore, if the internal iterations at a load step converge too slowly, or do not converge at all, then the load step should be reduced to decrease the spectral radius. We have found that simple load bisection algorithms, i.e. those bisecting the load step size when, within a load step, the number of global/local iterations exceeds a limit, to be quite robust and successful in reducing computations while maintaining accuracy and convergence.

3. Numerical experiments

We considered a sample of porous aluminum ($\kappa_1 = 77.9$ GPa, $\mu_1 = 24.9$ GPa), which obeys a J_2-flow rule with $C_2 = 0$. Specifically, yield is initiated when $(g(\boldsymbol{\sigma}) : g(\boldsymbol{\sigma}))^{\frac{1}{2}} = \sqrt{\boldsymbol{\sigma}' : \boldsymbol{\sigma}'} = 40$ MPa $= \mathcal{K}$. In the incremental simulations, the load step size was set to initially 20 displacement controlled strain increments to guide the following multiaxial load history, $\mathcal{E}_{ij} = 0 \rightarrow 0.0005$. At the selected value of yield stress, the pure solid aluminum material will yield at approximately $\|\mathcal{E}\| = 0.00033$. The response was invariant beyond this number of load steps. For the response to be considered macroscopically reliable, the size of the sample must be enlarged until the

response is invariant. In the voids, the material was set to nearly zero values ($\kappa_1 = 0.0001$ Pa, $\mu_1 = 0.0001$ Pa). We controlled the volume fraction of pores via a pore/sample size ratio. We defined a subvolume size $V \stackrel{\text{def}}{=} \frac{L \times L \times L}{N}$, where N is the number of pores in the entire sample and where L is the length of the (cubical $L \times L \times L$) sample, and a radius r, of a single particle. The ratio between the diameter and the subvolume was a control parameter defined by $\zeta \stackrel{\text{def}}{=} \frac{r}{V^{\frac{1}{3}}}$. A uniform mesh was used, as in the simulations, in conjunction with a standardglobal/local return mapping algorithm. The finite element meshes were repeatedly refined, and a mesh density of $9 \times 9 \times 9$ trilinear hexahedra (approximately 2200–3000 degrees of freedom) *per particle* was found to deliver invariant macroscopic responses. A "2/5" Gauss rule was used, whereby element with discontinuities had increased Gauss rules ($5 \times 5 \times 5$) to increase the resolution of the internal geometry, while elements with no discontinuities had the nominal $2 \times 2 \times 2$ rule. During the numerical experiments, the samples were successively enlarged, i.e. containing more pores, until the macroscopic responses showed little variation for further enlargements. Samples containing virtually 20 pores delivered approximately invariant results. The macroscopic response results are shown in Fig. 1 for various pore volume fractions. Table 1 depicts a numerically generated macroscopic stress reduction factor (R^{FEM}), due to the pores, defined by $R^{\text{FEM}} = \frac{\| \langle \boldsymbol{\sigma}'^{\text{FEM}} \rangle_\Omega \|}{\| \langle \boldsymbol{\sigma}'^{0} \rangle_\Omega \|}$, where $\left\| \langle \boldsymbol{\sigma}'^{\text{FEM}} \rangle_\Omega \right\| \stackrel{\text{def}}{=} \sqrt{\langle \boldsymbol{\sigma}'^{\text{FEM}} \rangle_\Omega : \langle \boldsymbol{\sigma}'^{\text{FEM}} \rangle_\Omega}$, and where $\langle \boldsymbol{\sigma}'^{0} \rangle_\Omega$ was the yield stress in the nonporous solid. The $\boldsymbol{\sigma}'^{\text{FEM}}$ is generated by the finite element computations for the porous solid. For more details on such simulation techniques see Zohdi and Wriggers (2001). The sequence in Fig. 2 (for 15% pore volume fraction) suggests that the *macroscopic response appears linearly elastic up until the "plastic pockets" between the pores connect*. Until they connect,

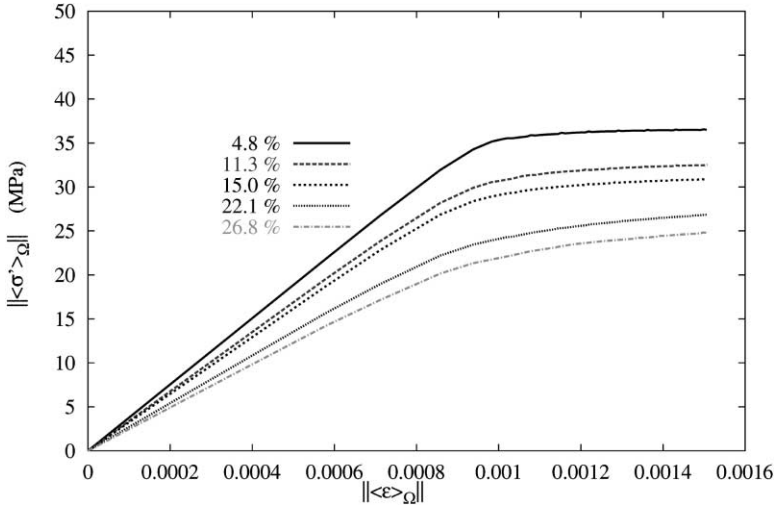

Fig. 1. Elasto-plastic finite element simulation (46875 DOF) of a sample of aluminum embedded with 20 pores occupying approximately 4.8, 11.3, 15.0, 22.1 and 26.8% of the volume.

Table 1
Numerically generated macroscopic yield stress reduction factors

ζ	v_2	$1-v_2$	R^{FEM}	$\frac{(1-v_2)}{R^{\mathrm{FEM}}}$
0.225	0.048	0.952	0.941	1.012
0.300	0.113	0.887	0.888	0.999
0.320	0.150	0.850	0.841	1.011
0.375	0.221	0.779	0.777	1.003
0.400	0.268	0.732	0.744	0.984

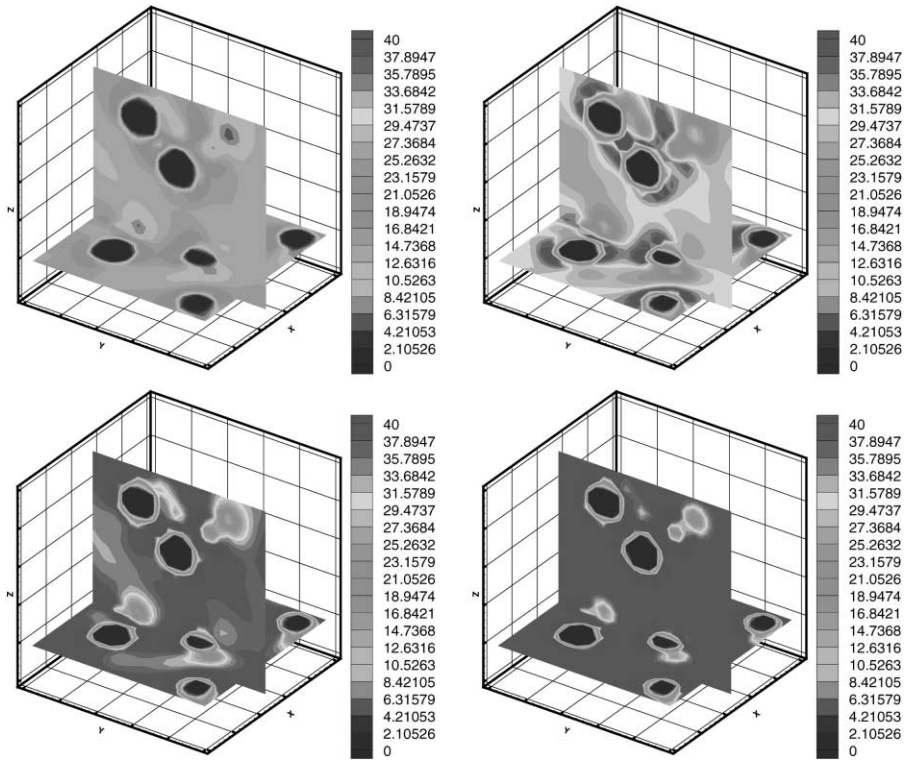

Fig. 2. SPHERES/PORE VOLUME FRACTION = 15%: Successive frames of $\|\boldsymbol{\sigma}'\|$ (MPa) for load levels of $\mathcal{E} = 0.0001$, 0.0002, 0.0003 and 0.004. Remark: The yellow rings that appear around the particles occur due to the fact that the average values are plotted *per finite element*.

the macroscopic secant modulus remains relatively insensitive to the localized yielding, i.e. the material behaves as if it were linearly elastic. It appears that the macroscopic strain at which the "point of connection" occurs, and the macroscopic strain at which a completely plasticized matrix occurs, are quite close, as hypothesized by Sevostianov and Kachanov (2001). As a consequence, the reduction of the macro-

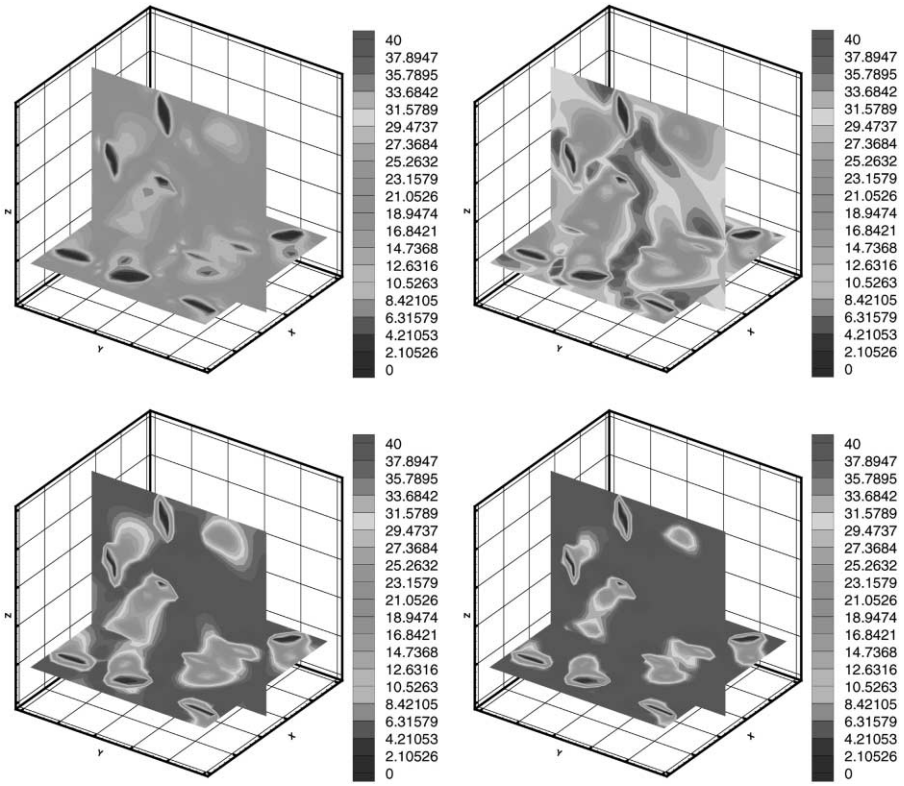

Fig. 3. ELLIPSOIDS/PORE VOLUME FRACTION = 6.9%: Successive frames of $\|\boldsymbol{\sigma}'\|$ (MPa) for load levels of $\mathcal{E} = 0.0001$, 0.0002, 0.0003 and 0.0004.

scopic poroplastic yield stress is approximated quite closely by $1-v_2$ times the dense nonporous yield stress, where v_2 is the volume fraction of the pores, since $\langle \boldsymbol{\sigma} \rangle_{\Omega} = v_1 \langle \boldsymbol{\sigma} \rangle_{\Omega_1} + v_2 \langle \boldsymbol{\sigma} \rangle_{\Omega_2} = v_1 \langle \boldsymbol{\sigma} \rangle_{\Omega_1} = (1 - v_2) \langle \boldsymbol{\sigma} \rangle_{\Omega_1} = (1 - v_2)\boldsymbol{\sigma}^0$, where $\boldsymbol{\sigma} = \mathbf{0}$ in the pores. This result holds for any part of the stress, in particular for $\boldsymbol{\sigma}'$. The quality of the hypothesis of Sevostianov and Kachanov (2001) can be directly related to the value of a reduction factor, since in the ideal case, $(1 - v_2)\boldsymbol{\sigma}'^{,0} = R^{\mathrm{FEM}}\boldsymbol{\sigma}'^{,0}$. Since $(1\text{-}v_2)/R^{\mathrm{FEM}} \approx 1$, as shown in Table 1, the hypothesis of Sevostianov and Kachanov (2001) is quite accurate. Such tests were repeated for various matrix materials, with the results being qualitatively the same. Furthermore, this finding appears to be insensitive to pore shape. As a further example, the same aluminum matrix [$(\kappa, \mu) = (77.9, 24.9$ GPa)] embedded with 20 randomly distributed oblate ellipsoidal pores with aspect ratio set to $AR = 0.3 = \frac{r_1}{r_2}$, where $r_2 = r_3$. The same size value, $\zeta = 0.375$, was used for the largest radii (r_2 and r_3), which resulted in a volume fraction of approximately 7%. Fig. 3 illustrates the similarity of the plastic flow to that of the spherical pore case.

4. Conclusions

The results presented in Figs. 2 and 3 show that the transition from the macroscopically linear (''elastic'') behavior to macroscopic plastic yield occurs in a very narrow loading interval, up to porosity levels of approximately 20%. This makes it possible to idealize this interval as a point and, thus, to identify a yield surface in the stress space. We emphasize that these results are obtained under the assumption that the material is perfectly plastic, i.e. experiences no noticeable hardening (at least at the initial ''plateau'' stage of plasticity), as is relevant, for example, for aluminum. The strain level at yield is independent of porosity and is a constant for a given matrix material, which is consistent with the cited experimental observations. This confirms the hypothesis of Sevostianov and Kachanov (2001) that, in turn, makes it possible to express the yield surface as an explicit function of the porous space geometry. It is observed that ''plastic percolation'' occurs within a very narrow interval of applied stresses/strains. We note that this observation is fully consistent with results of numerical/experimental studies of plastic percolation in GASAR materials (Kee et al., 1998), where the percolation occurred when over 80% of the material was plasticized.

References

Da, Silva, M.G., Ramesh, K.T., 1997a. The rate-dependent deformation and localization of fully dense and porous Ti-6Al-4V. Material Science and Engineering A232, 11–22.

Da, Silva, M.G., Ramesh, K.T., 1997b. The rate-dependent deformations of porous pure iron. The International Journal of Plasticity 13, 587–610.

Everett, R.K., 1998. Method for Forming Porous Metals. US Patent No 5930580; 27 July.

Green, R.J., 1972. A plasticity theory for porous solids. International Journal of Mechanical Science 14, 215–224.

Gu, C., Kim, L., Anand, L., 2001. Constitutive equations for metal powders: application to powder forming processes. The International Journal of Plasticity 17, 147–209.

Gurson, A.L., 1977. Continuum theory for ductile rupture by void nucleation and growth: part I—yield criteria and flow rules for porous media. Journal of Engineering Materials and Technology 99, 2–15.

Horstmeyer, M.F., Matalanis, M.M., Sieber, A.M., Botos, M.L., 2000. Micromechanical finite element calculations of temperature and void configuration effects on void growth and coalesence. The International Journal of Plasticity 16, 979–1015.

Kachanov, M., Tsukrov, I., Shafiro, B., 1994. Effective moduli of solids with cavities of various shapes. Applied Mechanics Reviews 47 (1), S151–S174.

Kee, A., Matic, P., Everett, R.K., 1998. A mesoscale computer simulation of multiaxial yield in GASAR porous copper. Material Science and Engineering A249, 30–39.

Khan, A., Huang, S. 1995. Continuum Theory of Plasticity. John Wiley.

Khan, A.S., Zhang, H., 2000. Mechanically alloyed nanocrystalline iron and copper mixture: behavior and constitutive modeling over a wide range of strain rates. The International Journal of Plasticity 16, 1477–1492.

Kharaishi, T.A., Khaleel, M.A., Zbib, H.M., 2001. A parametric experimental study of void growth in superplastic deformation. The International Journal of Plasticity 17, 315–317.

Kuhn, H.A., Downey, C.L., 1971. Deformations characteristics and plasticity theory for sintered powder materials. International Journal of Powder Metallurgy 3, 63–73.

Lee, Y.K., 1988. A finite elastoplastic flow theory for porous media. The International Journal of Plasticity 4, 301–316.

Lee, B.J., Mear, M., 1991. On the yield strength of metals containing spheroidal inclusions or voids. Mechanics of Materials 12, 191–205.

Mähler, L., Ekh, M., Runnesson, K., 2001. A class of hyperelastic-viscoplastic models for porous materials: theory and numerics. The International Journal of Plasticity 17, 943–969.

Mear, M., 1990. On the plastic yielding of porous materials. Mechanics of Materials 9, 33–48.

Olevsky, E., 1998. Theory of sintering: from discrete to continuum. Material Science and Engineering R23, 41–100.

Nagayaki, S., Goya, M., Sowerby, R., 1993. The influence of void distribution on the yielding. The International Journal of Plasticity 9, 199–212.

Pardoen, T., Hutchinson, J.W., 2000. An extended model for void growth and coalescence. Journal of Mechanics Physics Solids 48, 2467–2512.

Qui, Y.P., Weng, G.J., 1993. Plastic potential and yield function of porous materials with aligned and randomly oriented spherical voids. The International Journal of Plasticity 9, 271–290.

Sevostianov, I., Kachanov, M., 2001. On the yield condition for anisotropic porous materials. Material Science and Engineering A313, 1–15.

Shapovalov, V.I., 1993. Method for Manufacturing Porous Articles, US Patent No. 5181549, 26 January 1993.

Shapovalov, V.I., Timchenko, A.G., 1993. Peculiarities of gas-crystal structure formation in aluminum and its alloys in presence of hydrogen. Physics of Metals 76, 335–337.

Shima, S., Oyane, M., 1976. Plasticity theory for porous metals. International Journal of Mechanical Science 18, 285–291.

Shtern, M., 1981. On governing equations for powder and porous bodies. Soviet Powder Metallurgy and Metal Ceramics 28, 31–35.

Skorokhod, V., 1965. Mean square stress and strain rate for porous materials. Soviet powder metallurgy and metal ceramics 12, 31–35.

Yee, K.C., Mear, M., 1996. Effect of void shape on the macroscopic response of nonlinear solids. The International Journal of Plasticity 12, 35–43.

Wang, Z.C., Davies, T.J., Ridley, N., Ogwu, A.A., 1996. Superplasticity of ceramic materials—II. Effect of initial porosity and doping on the superplastic behaviour of alumina. Acta Materialia 44, 4301–4309.

Zohdi, T.I., Wriggers, P., 2001. A model for simulating the deterioration of structural-scale material responses of microheterogeneous solids. Computer Methods in Applied Mechanics and Engineering 190, 22–23. 2803–2823.